Multidisciplinary Design Optimization for Vibration Control of Smart Laminated Composite Structures

Shinya HONDA, Itsuro KAJIWARA, and Yoshihiro NAIRTA

Faculty of Engineering, Hokkaido University

N13W8, Kita-ku, Sapporo, 060-8628, Hokkaido, Japan

ABSTRACT

The structure and vibration control system of smart laminated composites consisting of graphite-epoxy composites and piezoelectric actuators are designed for optimum vibration suppression. The placement of piezoelectric actuators, the lay-up configurations of laminated composite plates and the H_2 control system are employed as design variables and they are optimized simultaneously by a simple genetic algorithm (SGA). To reduce complexity, only pre-selected families of lay-up configurations are considered. An objective function is the H_2 performance with respect to the controlled response for vibration suppression. A multidisciplinary design optimization is performed with the above three design variables and then the output feedback system is reconstructed with a dynamic compensator based on a linear matrix inequality (LMI) approach. The validity of the modeling and calculation technique is confirmed experimentally. Optimization results show that optimized smart composites with the present approach successfully realize vibration suppression and it is confirmed that the proposed multidisciplinary design optimization technique enhances the vibration suppression of smart composites.

Key Words: vibration control, laminated composite, robust control, piezoelectric, modal transformation, optimization, genetic algorithm

INTRODUCTION

Advantages of advanced composite materials in industrial use are becoming increasingly obvious. Among types of composites, laminated fibrous composites are finding a wide range of applications in structural design, especially for light-weight structures that have strict stiffness and strength requirements. In many applications, light-weight structures are typically exposed to severe vibration environments, and vibration suppression of composites is becoming increasingly important. A smart composite with a piezoelectric (PZT) actuator and sensor is an effective solution to suppress structural vibration, and in this study, structures and control systems of smart laminated composites are designed for optimum vibration suppression.

The performance of vibration control of structures strongly depends on the location of actuators as the optimum placement of actuators results in activating control forces effectively in the structures. Many studies on this problem have been reported: Quek, Wang and Ang (2003) proposed an optimization technique for the placement of PZT actuators and sensors to suppress the vibration of composite plates using a pattern search method. Jha and Inman (2003) determined optimum placements and sizes of actuators and sensors using a genetic algorithm (GA) method for inflated torus structures. Ono, Kajiwara and Ishizuka (2007) developed a simultaneous optimization method for actuator placements and H_2 control systems to suppress plate vibration with a finite element analysis (FEA) and sound pressure levels with a boundary element method (BEM). Rader et al. (2007) presented an approach to optimizing the placement of piezoelectric actuators considering different numbers of actuators for the vibration control of a flexible aircraft fin. Rao et al. (2008) employed a particle swarm based evolutionary optimization technique for optimization of actuator placement to improve H_∞ control performance. Kang and Tong (2008) optimized the topologies of PZT actuators and control voltage simultaneously by a method of moving asymptotes. Kajiwara, Takahashi and Arisaka (2009) applied an actuator placement technique to the arm of hard disk drives to enhance the servo bandwidth of the head positioning system. However, the above studies limited the controlled objects to isotropic structures or anisotropic composites with pre-established lay-up configurations.

Laminated composites can be tailored by varying the stacking sequences of the fiber orientation angles in each layer and/or layer thickness. Generally, laminated composites are created by stacking orthotropic layers termed *lamina* with different fiber orientation angles. The mechanical properties of laminated composites depend on the lay-up configurations and it is possible to design vibration characteristics of the plate arbitrarily by arranging fiber orientation angles. The use of lamination parameters (Gürdal, Haftka and Hajela, 1999) which describe equivalent stiffnesses for the through-thickness of plates in a simple form is an effective approach towards an optimization of lay-up configurations, but it requires a two-step optimization process to obtain the practical lay-up configurations or fiber orientation angles in each layer, and deriving a lay-up configuration corresponding to the parameters is not straightforward. Fukunaga, Sekine and Sato (1992) proposed an optimization method to maximize the fundamental frequency using lamination parameters. They first determined optimum parameters with a mathematical programming method and then the corresponding lay-up configuration for the parameters were derived by a graphical method. Autio (2000) used a GA to determine the lay-up corresponding to the lamination parameters. Honda, Narita and Sasaki (2009) presented an effective method for converting lamination parameters to lay-up configurations by dividing a laminate into sub-domains. Matsuzaki and Todoroki (2007) proposed an optimization technique using a fractal branch-and-bound method for the lamination parameters. Meanwhile, optimization techniques of laminated composites without lamination parameters have been also proposed to avoid two-step optimization. Riche and Haftka (1993) maximized buckling loads of laminated composite plates using a GA, directly assigning fiber orientation angles in each layer as a design variable. Narita (2003) proposed a layerwise optimization (LO) method and determined fiber orientation angles sequentially from the outermost to the innermost layers. The objectives of these studies have been to maximize the fundamental frequencies or buckling loads of the laminated composites. However, it is becoming increasingly difficult to satisfy the strict vibration requirements for laminated composites in recent advanced mechanical structures by only structural design, and thus smart composites with active vibration control is a promising approach to improving the vibration properties of mechanical structures.

An optimization method is proposed here to improve the active vibration control performance of smart laminated composites. In the optimization problem, the fiber orientation angles and their stacking sequences are

determined multidisciplinary with PZT actuator placement and control system to enhance vibration suppression of the smart structures. As mentioned above, many studies have reported optimization of lay-up configurations and actuator placements separately for smart composites, but no study has optimized both the lay-up configurations and the actuator placements simultaneously. In the approach here, the smart composite is modeled by finite elements and the order of the model is reduced by modal coordinate transformation. The vibration control system is designed by solving the H_2 control problem using a reduced-order modal model. The multidisciplinary design optimization is performed with respect to the smart composite by a simple genetic algorithm method (SGA) assuming the state feedback and then the output feedback system is reconstructed based on the linear matrix inequality (LMI) approach. The experimental results prove the validity of the proposed approach on the multidisciplinary design optimization, and the numerical results show that the obtained composite plates with optimum lay-ups, actuator placements and control systems provide better suppression of the vibration response than plates with other lay-up configurations.

ANALSYS AND OPTIMIZATION METHOD

Stiffnesses of Laminated Composites

A symmetric K-layered plate with respect to the middle surface as shown in Figure 1 is considered here. The plate dimensions are $a \times b \times h$ (h: thickness), where h is thin enough to satisfy the plane stress condition. The fiber direction and the direction normal to the fibers in the kth layer are defined as 1 and 2, respectively. The stress-strain relation in the direction of the material principal axis is given by

$$\begin{Bmatrix} \sigma_1 \\ \sigma_2 \\ \tau_{12} \end{Bmatrix} = \begin{bmatrix} Q_{11} & Q_{12} & 0 \\ Q_{12} & Q_{22} & 0 \\ 0 & 0 & Q_{66} \end{bmatrix} \begin{Bmatrix} \varepsilon_1 \\ \varepsilon_2 \\ \gamma_{12} \end{Bmatrix} \tag{1}$$

where Q_{ij} (i, j = 1, 2, 6) are stiffness coefficients defined by the material constants in the direction of the material principal axis.

$$
\begin{aligned}
&Q_{11} = E_1/(1-\nu_{12}\nu_{21}), \quad Q_{22} = E_2/(1-\nu_{12}\nu_{21}),\\
&Q_{12} = \nu_{21}Q_{11} = \nu_{12}Q_{22}, \quad Q_{66} = G_{12}
\end{aligned} \tag{2}
$$

Here, E_1 and E_2 are the moduli of elasticity in the fiber and normal to the fiber direction, G_{12} is the shear modulus, and ν_{12} and ν_{21} are the major and minor Poisson ratios. Rotating the axis systems in Fig. 1 by an amount θ_k, the fiber orientation angle in the kth layer defined from the x axis in the counterclockwise direction gives the stress-strain relation with respect to the O-xy coordinates.

$$
\begin{Bmatrix} \sigma_x \\ \sigma_y \\ \tau_{xy} \end{Bmatrix} = \begin{bmatrix} \overline{Q}_{11} & \overline{Q}_{12} & \overline{Q}_{16} \\ \overline{Q}_{12} & \overline{Q}_{22} & \overline{Q}_{26} \\ \overline{Q}_{16} & \overline{Q}_{26} & \overline{Q}_{66} \end{bmatrix} \begin{Bmatrix} \varepsilon_x \\ \varepsilon_y \\ \gamma_{xy} \end{Bmatrix} \tag{3}
$$

where $\overline{Q}_{ij}$ $(i, j = 1, 2, 6)$ are the transformed stiffness coefficients. With material invariants U_i $(i = 1, 2, \ldots 5)$, they are given by

$$
\begin{Bmatrix} \overline{Q_{11}} \\ \overline{Q_{22}} \\ \overline{Q_{12}} \\ \overline{Q_{66}} \\ \overline{Q_{16}} \\ \overline{Q_{26}} \end{Bmatrix} = \begin{bmatrix} U_1 & \cos\theta_k & \cos 4\theta_k \\ U_1 & -\cos\theta_k & \cos 4\theta_k \\ U_4 & 0 & -\cos 4\theta_k \\ U_5 & 0 & -\cos 4\theta_k \\ 0 & (\sin 2\theta_k)/2 & \sin 4\theta_k \\ 0 & (\sin 2\theta_k)/2 & -\sin 4\theta_k \end{bmatrix} \begin{Bmatrix} 1 \\ U_2 \\ U_3 \end{Bmatrix} \tag{4}
$$

and U_i are

$$
\begin{Bmatrix} U_1 \\ U_2 \\ U_3 \\ U_4 \\ U_5 \end{Bmatrix} = \begin{bmatrix} 3/8 & 3/8 & 1/4 & 1/2 \\ 1/2 & -1/2 & 0 & 0 \\ 1/8 & 1/8 & -1/4 & -1/2 \\ 1/8 & 1/8 & 3/4 & -1/2 \\ 1/8 & 1/8 & -1/4 & 1/2 \end{bmatrix} \begin{Bmatrix} Q_{11} \\ Q_{22} \\ Q_{12} \\ Q_{66} \end{Bmatrix} \tag{5}
$$

The relations between the resultant stress-strain and the resultant moment-curvature are obtained by a through-thickness integration of Equation (3). The plate is limited to symmetrically laminated plates here and so the in-plane and out-of-plane coupling is cancelled. Then, the in-plane stiffnesses A_{ij} and the out-of-plane stiffnesses D_{ij} $(i, j = 1, 2, 6)$ can be considered independently. With z_k, which is the z coordinate of the outer surface of the kth layer, A_{ij} and D_{ij} are expressed by

$$\left.\begin{aligned} A_{ij} &= \sum_{k=1}^{K} (\overline{Q_{ij}})_k (z_k - z_{k-1}) \\ D_{ij} &= \frac{1}{3}\sum_{k=1}^{K} (\overline{Q_{ij}})_k (z_k^3 - z_{k-1}^3) \end{aligned}\right\} \tag{6}$$

In the finite element analysis, the element stiffness is defined using the stiffnesses in Equation (6) and the frequencies and modal vectors depend on A_{ij} and D_{ij}.

Modeling of Smart Structures

Finite element analysis (FEA) is used to model smart structures and the order of the finite element model is reduced with the modal analysis technique. The finite element model of the composite plate here is shown in Figure 2. The plate right edge is clamped and the dimensions of the plate are $a \times b \times h = 200 \times 160 \times 2$ mm with $10 \times 8 = 80$ elements. The locations for an accelerometer and an impulse (disturbance) input are also shown in Figure 2. The lay-up configurations of laminated composites are limited to symmetric eight layers $[\theta_1/\theta_2/\theta_3/\theta_4]$s where θ_1 is the angle in the outermost layer. The general purpose FEA software (ANSYS 11.0) is used with the linear layered structural shell element (SHELL99) for the modeling of the plate, SHELL99 is a quadratic element and the number of nodes in the model here is 277. Assuming graphite/epoxy (CFRP) composite, the material constants are: $E_1 = 141$ GPa, $E_2 = 10.0$ GPa, $G_{12} = 7.17$ GPa, $\nu_{12} = 0.28$ and $\rho = 1600$ kg/m^3. Properties of PZT actuator are listed in Table 1. The actuators have 0.5 mm thickness and 15 mm width but their mass and stiffness effects are neglected in the modeling since they are thin enough compared with CFRP plate, and they are assumed as segments of line and input points of control forces at their end points.

The equation of motion for an n degree-of-freedom system is expressed as

$$\mathbf{M}_s\ddot{\mathbf{x}} + \mathbf{C}_s\dot{\mathbf{x}} + \mathbf{K}_s\mathbf{x} = \mathbf{B}_{1s}\mathbf{w} + \mathbf{B}_{2s}\mathbf{u} \tag{7}$$

where $\mathbf{M}_s$ and $\mathbf{K}_s$ are the mass and stiffness matrixes; $\mathbf{C}_s$ is the assumed proportional viscous damping matrix; and $\mathbf{x}$, $\mathbf{w}$ and $\mathbf{u}$ are the displacement, disturbance and control input vectors, respectively. A finite element model is flexible and able to accommodate a wide range of shapes, as well as it is an effective modeling method, but it has a large number of degree-of-freedom. This results in heavy calculation loads in the design of control systems and

optimization process, and here the model is reduced by transforming the spatial coordinates to modal space. With the lowest r modes, the modal matrix $\mathbf{\Phi}$ is defined by

$$\mathbf{\Phi} = [\phi_1 \quad \phi_2 \quad \cdots \quad \phi_r] \tag{8}$$

where ϕ_i (i = 1, 2, …, r) are the mode vectors for each mode, normalized with respect to the mass matrix. These procedures are carried out by the FEA. Equation (7) is transformed to the reduced-order state-equation with the transformation $\mathbf{x} = \mathbf{\Phi}\boldsymbol{\xi}$.

$$\dot{\mathbf{q}} = \mathbf{A}\mathbf{q} + \mathbf{B}_1\mathbf{w} + \mathbf{B}_2\mathbf{u} \tag{9}$$

where

$$\begin{aligned} \mathbf{q} &= \begin{Bmatrix} \boldsymbol{\xi} \\ \dot{\boldsymbol{\xi}} \end{Bmatrix} \qquad \mathbf{A} = \begin{bmatrix} \mathbf{0} & \mathbf{I}_r \\ -\mathbf{\Lambda} & -\mathbf{\Phi}^{\mathrm{T}}\mathbf{C}_s\mathbf{\Phi} \end{bmatrix} \\ \mathbf{B}_1 &= \begin{bmatrix} \mathbf{0} \\ \mathbf{\Phi}^{\mathrm{T}}\mathbf{B}_{1s} \end{bmatrix} \quad \mathbf{B}_2 = \begin{bmatrix} \mathbf{0} \\ \mathbf{\Phi}^{\mathrm{T}}\mathbf{B}_{2s} \end{bmatrix} \end{aligned} \tag{10}$$

The $\mathbf{\Lambda}$ is the diagonal eigenvalue matrix expressed by

$$\mathbf{\Lambda} = \mathrm{diag}[\Omega_1^2 \quad \Omega_2^2 \quad \cdots \quad \Omega_r^2] \tag{11}$$

with Ω_i (i = 1, 2, …, r) the undamped natural frequencies of the structure. Using a modal damping ratio ζ_i (i = 1, 2, …, r) for each mode, $\mathbf{\Phi}^{\mathrm{T}}\mathbf{C}_s\mathbf{\Phi}$ is denoted by

$$\mathbf{\Phi}^{\mathrm{T}}\mathbf{C}_s\mathbf{\Phi} = \mathrm{diag}[2\varsigma_1\Omega_1 \quad 2\varsigma_2\Omega_2 \quad \cdots \quad 2\varsigma_r\Omega_r] \tag{12}$$

$\mathbf{B}_{2s}$ in Equations (7) and (10) is determined by the relationship between the control input $\mathbf{u}$ and the moment induced by the piezoelectric actuator.

The output equation of the system can be expressed by

$$\mathbf{y}_2 = \mathbf{C}_2\mathbf{q} + \mathbf{D}_{21}\mathbf{w} + \mathbf{D}_{22}\mathbf{u} \tag{13}$$

Acceleration is employed as the feedback signal and is detected by the accelerometer in the system. Substituting the transformation equation $\mathbf{x} = \mathbf{\Phi}\boldsymbol{\xi}$ into Equation (9) yields the modal acceleration

$$\ddot{\boldsymbol{\xi}} = -\mathbf{\Phi}^{\mathrm{T}}\mathbf{C}_s\mathbf{\Phi}\dot{\boldsymbol{\xi}} - \mathbf{\Lambda}\boldsymbol{\xi} + \mathbf{\Phi}^{\mathrm{T}}\mathbf{B}_{1s}\mathbf{w} + \mathbf{\Phi}^{\mathrm{T}}\mathbf{B}_{2s}\mathbf{u} \tag{14}$$

The detected acceleration can be expressed by

$$\mathbf{y}_a = \mathbf{C}_a \ddot{\mathbf{x}} \tag{15}$$

Using Equations (14) and (15), the coefficient matrixes in Equation (13) are

$$\begin{aligned} &\mathbf{C}_2 = \mathbf{C}_a \boldsymbol{\Phi}[-\boldsymbol{\Lambda} \quad -\boldsymbol{\Phi}^{\mathrm{T}} \mathbf{C}_s \boldsymbol{\Phi}], \\ &\mathbf{D}_{21} = \mathbf{C}_a[\mathbf{0} \quad \boldsymbol{\Phi}]\mathbf{B}_1, \quad \mathbf{D}_{22} = \mathbf{C}_a[\mathbf{0} \quad \boldsymbol{\Phi}]\mathbf{B}_2 \end{aligned} \tag{16}$$

Design of Control System

The block diagram of the control system is shown in Figure 3, $\mathbf{P}(s)$ is the controlled object and $\mathbf{K}(s)$ is the dynamic compensator working as the controller. The controller $\mathbf{K}(s)$ is obtained by solving the H_2 control problem

$$\min. \left\| \mathbf{T}_{y1w} \right\|_2 \tag{17}$$

where $\mathbf{T}_{y1w}$ is the transfer function matrix between the disturbance $\mathbf{w}$ and the controlled variable $\mathbf{y}_1$ which is described as

$$\mathbf{y}_1 = \begin{Bmatrix} \mathbf{Q}^{1/2} \mathbf{z}_1 \\ \mathbf{R}^{1/2} \mathbf{u} \end{Bmatrix} \tag{18}$$

here $\mathbf{z}_1$ is the controlled response, and $\mathbf{Q}$ and $\mathbf{R}$ are weight parameters for the controlled response $\mathbf{z}_1$ and control input $\mathbf{u}$, respectively. Using Equation (18), the control problem in Equation (17) becomes equivalent to the control problem for a white noise disturbance.

$$\min. E\left[\mathbf{z}_1^{\mathrm{T}} \mathbf{Q} \mathbf{z}_1 + \mathbf{u}^{\mathrm{T}} \mathbf{R} \mathbf{u}\right] \tag{19}$$

where $E[*]$ is the expected value. $\mathbf{z}_1$ is defined in the modal coordinates and modal control is applied in this study.

In the modal control problem, $\mathbf{z}_1$ is comprised of the modal coordinates and formulated as

$$\mathbf{z}_1 = \mathbf{W}_{10} \mathbf{q} \tag{20}$$

with the modal weighting matrix $\mathbf{W}_{10}$ defined by

$$\mathbf{W}_{10} = \mathrm{diag}[w_1 \quad w_2 \quad \cdots \quad w_{2r}] \tag{21}$$

Weighting each modal coordinate with each coefficient simply achieves the modal shaping and makes it possible to suppress the target mode vibration effectively. With Equations (18) and (20), the controlled variable $\mathbf{y}_1$ is expressed as

$$\mathbf{y}_1 = \mathbf{C}_1\mathbf{q} + \mathbf{D}_{12}\mathbf{u} \tag{22}$$

with $\mathbf{C}_1$ and $\mathbf{D}_{12}$:

$$\mathbf{C}_1 = \begin{bmatrix} \mathbf{Q}^{1/2}\mathbf{W}_{10} \\ \mathbf{0} \end{bmatrix}, \quad \mathbf{D}_{12} = \begin{bmatrix} \mathbf{0} \\ \mathbf{R}^{1/2}\mathbf{I} \end{bmatrix} \tag{23}$$

The optimum control law with the control problem (17) or (19) is obtained as a form of state feedback:

$$\mathbf{u} = -\mathbf{F}\mathbf{q} \tag{24}$$

The optimum feedback gain $\mathbf{F}$ is

$$\mathbf{F} = -\mathbf{R}^{-1}\mathbf{B}_2^{\mathrm{T}}\mathbf{P} \tag{25}$$

where $\mathbf{P}$ is the solution of the Riccati equation:

$$\mathbf{A}^{\mathrm{T}}\mathbf{P} + \mathbf{P}\mathbf{A} + \mathbf{W}_{10}^{\mathrm{T}}\mathbf{Q}\mathbf{W}_{10} - \mathbf{P}\mathbf{B}_2\mathbf{R}^{-1}\mathbf{B}_2^{\mathrm{T}}\mathbf{P} = 0 \tag{26}$$

The performance indexes with respect to the controlled response and the control input are

$$H_{\mathbf{z}1} = E\left[\mathbf{z}_1^{\mathrm{T}}\mathbf{z}_1\right], \quad H_{\mathbf{u}} = E\left[\mathbf{u}^{\mathrm{T}}\mathbf{u}\right] \tag{27}$$

These performance indexes can be calculated by

$$H_{\mathbf{z}1} = \mathrm{trace}[\mathbf{C}_{10}\mathbf{X}\mathbf{C}_{10}^{\mathrm{T}}], \quad H_{\mathbf{u}} = \mathrm{trace}[\mathbf{F}\mathbf{X}\mathbf{F}^{\mathrm{T}}] \tag{28}$$

where $\mathbf{X}$ is the solution of the Lyapunow equation:

$$\mathbf{X}\mathbf{G}^{\mathrm{T}} + \mathbf{G}\mathbf{X} + \mathbf{B}_1\mathbf{B}_1^{\mathrm{T}} = 0 \tag{29}$$

where $\mathbf{G} = \mathbf{A} - \mathbf{B}_2\mathbf{F}$.

In an output feedback system, the output feedback law $\mathbf{u} = \mathbf{K}(s)\mathbf{y}$ is described as a state space form:

$$\begin{aligned} \mathbf{q}_{\mathbf{K}} &= \mathbf{A}_{\mathbf{K}}\mathbf{q}_{\mathbf{K}} + \mathbf{B}_{\mathbf{K}}\mathbf{y} \\ \mathbf{u} &= \mathbf{C}_{\mathbf{K}}\mathbf{q}_{\mathbf{K}} + \mathbf{D}_{\mathbf{K}}\mathbf{y} \end{aligned} \tag{30}$$

where the system matrixes $\mathbf{A}_{\mathbf{K}}$, $\mathbf{B}_{\mathbf{K}}$, $\mathbf{C}_{\mathbf{K}}$ and $\mathbf{D}_{\mathbf{K}}$ of the controller are designed with the LMI approach.

Multidisciplinary Design Optimization Problem

A multidisciplinary design optimization technique for smart composite structures is presented to enhance the closed-loop system performance in this study. Composite laminated plates are formed by thin orthotropic layers termed *lamina* and the vibration characteristics depend on the lay-up configuration. At the same time, the vibration control performance depends strongly on the actuator placement and the designed controller. The simultaneous optimization of the lay-up of composite, the placements of actuators and the control system will involve high control performances.

The optimization problem to achieve the above purpose is described by

$$\begin{aligned} &\text{Minimizing}: \quad J(\eta_L, \eta_c, \boldsymbol{\eta}_{\mathrm{AC}}) \\ &\text{Subject to:} \quad g_c^{\min} \le g_c(\eta_L, \eta_c, \boldsymbol{\eta}_{\mathrm{AC}}) \le g_c^{\max} \end{aligned}$$

The problem is defined to reduce the H_2 norm with respect to the controlled response, under the constraint of the H_2 norm with respect to the control input. From this, the objective function J to be minimized and the constraint function g_c depending on the design variables are defined as

$$J = H_{\mathbf{z}1}, \quad g_c = H_{\mathbf{u}} \tag{31}$$

where $H_{\mathbf{z}1}$ and $H_{\mathbf{u}}$ are the H_2 norms of the controlled response and control input, respectively, given by Equations (27) and (28). The design variables include the lay-up indexes η_L representing the lay-up configuration $[\theta_1/\theta_2/\theta_3/\theta_4]$s, the weighting coefficient η_c (= q_w) applied to the controlled response in the performance index for control system design and the actuator placements $\boldsymbol{\eta}_{\mathrm{AC}}$.

As an optimizer, a simple genetic algorithm (SGA) is employed with a two-point crossover, mutation and elitist tactics (Riche and Haftka, 1993). The design variables are coded by binary numbers for the SGA process and they are denoted as

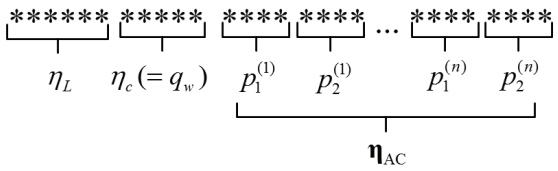

where * represents the binary numbers, 0 or 1. The actuators are assumed to be segments of lines in the calculation process and their placement is represented by

$$\boldsymbol{\eta}_{\mathrm{AC}} = \begin{bmatrix} p_1^{(1)} & p_2^{(1)} \\ p_1^{(2)} & p_2^{(2)} \\ \vdots & \vdots \\ p_1^{(n)} & p_2^{(n)} \end{bmatrix} \tag{32}$$

where $p_1^{(i)}$ and $p_2^{(i)}$ (i = 1, 2, …, n) are the nodes of end points of the ith actuator in the finite element model and n is number of actuators installed to the composites. An example of the actuator placement is suggested in Figure 4. The forces F applied by the actuators are linear to the input voltage u and calculated by $F = b_{2s}u$. The length of a PZT actuator is limited to $l \le l_{\max}$ (= 0.13 m). When the actuators cross each other, the design candidate has a penalty imposed on its objective function giving it a very high objective value in the minimizing problem.

Laminated plates with different lay-ups give different natural frequencies and modes, but performing the FEA repeatedly in the SGA process results in a heavy calculation load. To get around this, natural frequencies and modal matrixes for all possible lay-ups are calculated in advance and a database containing information of lay-up configurations and modal matrixes with lay-up indexes η_L is preliminarily developed. A design candidate with the lay-up index η_L refers to the database and the modal matrix corresponding to η_L is used to calculate the objective function by passing the FEA in the optimization process. The use of a database makes it possible to adapt the quality of solutions to the aim of the optimization. If the elements in the database are limited to commonly used lay-ups such as angle-ply, cross-ply and quasi-isotropic laminates, practical optimum solutions would be obtained. Using fine increments for the orientation angle in each layer will result in solutions with higher controlled performance than practical solutions since the problem has more degree-of-freedom than problem with a limited number of possible solutions.

It is necessary to design the output feedback controller in each step of the SGA, but calculating the feedback control law in every step also results in low calculation efficiency. The output feedback system is designed after carrying out the simultaneous optimization where it is assumed that all states of the structures can be observed and a state feedback is available. The present optimization process is configured to follow a three-step procedure and the flow chart of the optimization is shown in Figure 5.

[Step 1] Preparing the database containing natural frequencies and modal matrixes for all possible lay-up configurations by repeated application of the FEA.

[Step 2] Assuming the state feedback, $\mathbf{u} = -\mathbf{Fq}$, performing the simultaneous optimization for the lay-up configuration, the PZT actuator placement and the control system by the SGA.

[Step 3] Reconstructing the output feedback system with the dynamic compensator $\mathbf{K}(s)$ based on the LMI approach.

RESULTS AND DISCUSSION

Optimization Results with Commonly Used Lay-up Configurations

First, calculated results were obtained with the database composed of commonly used lay-ups where limited four fiber orientation angles 0°, 45°, -45° and 90° are used in the layer and a balanced rule constraint is imposed on lay-up configurations. Lay-ups have the same number of 45° and -45° layers to avoid the in-plane coupling between tensile and shearing deformation. The symmetric 8-layer plate $[\theta_1/\theta_2/\theta_3/\theta_4]$s is considered here and the number of possible lay-up configurations for the database becomes 70. Two actuators are installed here, the number of modes considered is the lowest eight, and the weight parameters **Q** and **R**, and the mode weight matrix $\mathbf{W}_{10}$ are defined as

$$\mathbf{Q}' = \mathbf{I}, \mathbf{R} = 10^2\mathbf{I},$$
$$\mathbf{W}_{10} = \mathrm{diag}[1 \quad 1 \quad 10^{-6} \quad 10^{-6} \quad 10^{-6} \quad 10^{-6} \quad 10^{-6} \quad 10^{-6}]$$

where the mode weights are imposed on the lowest two modes so as to suppress the first and second modes vibration.

The resulting optimal actuator placements are shown in Figure 6 where the plate right edge is clamped and the black strips represent the actuators and the design variable for control system q_w and resulting performance indexes H_{z1} are listed in Table 2. The optimum lay-up is [0/0/0/0]s and agrees with the lay-up giving the highest fundamental frequency for the cantilever plate. To confirm the validity of the optimization results, supplemental results for other plates with commonly used lay-ups, cross-ply [0/90/0/90]s, angle-ply [45/-45/45/-45]s and in-plane quasi-isotropic [0/45/-45/90]s are also shown in Figure 6 and Table 2. Here, other plates have their own optimum actuator placements and control variable q_w calculated by using the present approach but lay-ups are specified in advance and are not included in the design variables. All the ends of the actuators are adjacent to the clamped edges in Figure 6 and the lengths of all actuators are about 0.13 m ($\approx l_{\max}$). The H_2 norms with respect to the control input for all plates are $H_{\mathbf{u}} = 0.1 (= H_{\mathbf{u},\max})$. The [0/0/0/0]s plate indicates the lowest $H_{z1} = 6.76\times10^7$ of the four in Table 2 and this validates the optimization result.

Experimental Verification for the Present Technique

Calculated results are compared with experimental results to confirm the validity of the modeling and controller design techniques. Figure 7 is an outline of the experimental set up and Figure 8 shows the smart composite used in the vibration control experiment where the plate has the optimized [0/0/0/0]s lay-up and actuator placement shown in Figure 6.

The plate is excited by an impulse hammer and the acceleration signal is measured by an accelerometer. The feedback signal goes to a spectrum analyzer, and is also fed to a control PC with a control board through a low pass filter which passes a signal lower than 20 kHz. Then, the optimally designed digital controller in the control PC converts the feedback signal into the appropriate control input voltage, and the voltage amplified by a PZT driver is applied to the PZT actuators where the amplification factor is set to 30. The sampling frequency of the control system is 50 kHz.

Calculated and measured accelerances are indicated in Figure 9. The amounts of reduction in both the first and second peaks obtained in the experiments are about 10 dB, agreeing well with the calculated results although the magnitude is a little smaller than the calculated results. This shows that the modeling method including neglect of the PZT mass and stiffness effects and controller design techniques give valid results. The reduction of the magnitude of peaks means the increase of damping performance for the structure, invoking a smoothed phase-delay property in the vibration control frequency range. In Figure 9, compared with the results without control, smoothed phase-delay curves are found at the resonance peaks in the calculated result with control, and this is also seen for the experimental result with a little smoothness.

Optimization Results with Fine Increment Angles

The next optimization includes more degree-of-freedom for lay-up configurations and fine increment angles are employed to prepare the database. The symmetric 8-layer plate $[\theta_1/\theta_2/\theta_3/\theta_4]$s is considered and the increments in the fiber orientation angles are 15° for θ_1 and θ_2 (12 possible angle for each layer), and 45° for θ_3 and θ_4 (four possible angles) in the range of $-90° < \theta \leq 90°$ since the outer layers have a strong influence in determining the bending stiffness of laminated plates and also in the frequency responses. Put differently, the outer layers are considered more important to improve the control performance of the smart structures and they are assigned a larger number of degree-of-freedom for the optimum solution. The total number of possible lay-up configurations is $12^2 \times 4^2 = 2304$ and no constraints are imposed on the lay-up configurations.

The weight parameters **Q** and **R**, and the mode weight matrix $\mathbf{W}_{10}$ are defined for the lowest five modes as

$$\mathbf{Q} = \mathbf{I},\ \mathbf{R} = 10^2\mathbf{I},$$
$$\mathbf{W}_{10} = \mathrm{diag}[1 \quad 1 \quad 1 \quad 10^{-6} \quad 10^{-6}]$$

where the lowest three modes are weighted and controlled. The results are obtained for plates with the different numbers of actuators (AC = 1, 2, 3 and 4) where AC is the number of actuators. The optimum actuator placements are shown in Figure 10 and the obtained q_w, $H_{\mathbf{z}1}$, $H_{\mathbf{u}}$, and optimized lay-ups are listed in Table 3.

All plates display the same optimized lay-ups [-15/-15/0/-45]s, showing that the optimum lay-up is insensitive to the number of actuators with respect to vibration control, and the $H_{\mathbf{z}1}$ decreases as the number of actuators increases. As with the previous result which controls the lowest two modes, the [0/0/0/0]s plate also gives the lowest $H_{\mathbf{z}1} = 6.26\times10^{-7}$ among the commonly used lay-ups [0/0/0/0]s, [0/90/0/90]s, [45/-45/45/-45]s and [0/45/-45/90]s in the present problem suppressing the lowest three modes, and the optimized plate (AC = 2) gives $H_{\mathbf{z}1} = 4.42\times10^{-7}$. This is lower than the [0/0/0/0]s plate. The frequency characteristics for the [-15/-15/0/-45]s and [0/0/0/0]s plates with AC = 2 are shown in Figure 11. In addition to suppression of the first and second modes vibration, the third mode vibration is also suppressed well for the [-15/-15/0/-45]s plate compared with the [0/0/0/0]s plate. To show the reason for this, the lowest three vibration mode shapes of the plate with [-15/-15/0/-45]s and [0/0/0/0]s are shown in Figure 12 where the black lines (strips) show the actuators. The mode shapes of the plates with the optimized lay-up [-15/-15/0/-45]s are skewed, affected by the -15° fiber orientation angles in the outer two layers. Actuators for the plate with the optimum lay-up are arranged normal to the contour lines of the first vibration mode and cross the nodal lines in the second and third modes. Those of the [0/0/0/0]s plate are also arranged normal to the first and second modes but they do not cross the nodal lines of the third mode. This causes the superior vibration control performance of the plates with the optimum lay-up [-15/-15/0/-45]s. Laminated plates with different lay-ups invoke different mode shapes, and the simultaneous design of both the lay-up configuration (mode shape) and the actuator placement results in activating the control input effectively in the controlled structures. Therefore, it is concluded that the proposed multidisciplinary design optimization technique has advantages over the conventional technique for fixed lay-ups with respect to the vibration control of smart laminated composites.

CONCLUSIONS

The present study discussed a multidisciplinary design optimization of smart composite structures composed of laminated composites and piezoelectric actuators. The design variables were the lay-up configuration of composite plates, the placements of actuators and the control system based on the H_2 control specifications. The

controlled smart composite was modeled by finite elements and the order was reduced using a modal coordinate transformation technique. The simple genetic algorithm method was employed as a multidisciplinary design optimizer.

The validity of the calculation technique was confirmed by comparing calculated results with experimental results. The numerical results were for the plates with commonly used lay-ups and with lay-ups composed of fine increment angles. The plates with the optimized lay-ups provide better control performance in terms of vibration suppression than plates with other typical lay-ups. This allows the conclusion that the proposed multidisciplinary design optimization technique is effective for the design of smart laminated composite structures.

ACKNOWLEDGMENTS

This work was supported by KAKENHI (22760164), and the first author expresses gratitude to Mr. Satoshi Nakamura, who is a graduate student in Hokkaido University, for contributions to the experiments.

REFERENCES

Autio, M., 2000 "Determining the real lay-up of a laminate corresponding to optimal lamination parameters by genetic search," Structural and Multidisciplinary Optimization, 20: 301-310.

Fukunaga, H. and Sekine, H., 1992 "Stiffness design method of symmetric laminates using lamination parameters," AIAA Journal, 30(11): 2791-2793.

Gürdal, Z., Haftka, R. T. and Hajela, P., 1999, "Design and optimization of laminated composite materials," John Wiley & Sons, London

Honda, S., Narita, Y. and Sasaki, K. 2009, "Discrete optimization for vibration fesign of composite plates by using lamination parameters," Advanced Composite Materials, 18: 297-314.

Jha, A. K. and Inman, D. J, 2003, "Optimal sizes and placements of piezoelectric actuators and sensors for an inflated torus," Journal of Intelligent Material Systems and Structures, 14: 563-576.

Kajiwara, I., Takahashi, M. and Arisaka, T., 2009, "Optimization of smart structure for improving servo performance of hard disk drive," Journal of System Design and Dynamics, 3(6): 906-917.

Kang, Z. and Tong, L. 2008, "Integrated optimization of material layout and control voltage for piezoelectric laminated plates," Journal of Intelligent Material Systems and Structures, 19: 889-904.

Matsuzaki, R. and Todoroki, A., 2007, "Stacking-sequence optimization using fractal branch-and-bound method for unsymmetrical laminates," Composite Structures, 78: 537-550 (2007).

Narita, Y., 2003 "Layerwise optimization for the maximum fundamental frequency of laminated composite plate," Journal of Sound and Vibration, 263: 1005-1016.

Ono, K. Kajiwara, I. and Ishizuka, S. 2007, "Piezoelectric and control optimisation of smart structures for vibration and sound suppression," International Journal of Vehicle Design, 43(1/2/3/4): 184-199.

Quek, S. T., Wang, S. Y. and Ang, K. K. 2003, "Vibration control of composite plates via optimal placement of piezoelectric patches," Journal of Intelligent Material Systems and Structures, 14: 229-245

Rader, A. A., Afagh, F. F., Yousefi-Koma, A. and Zimcik, D. G., 2007, "Optimization of piezoelectric actuator configuration on a flexible fin for vibration control using genetic algorithms, " Journal of Intelligent Material Systems and Structures, 18: 1015-1033

Rao, A. K., Natesan, K., Bhat, M. S. and Ganguli, R., 2008, "Experimental demonstration of H∞ control based active vibration suppression in composite fin-tip of aircraft using optimally placed piezoelectric patch actuators," Journal of Intelligent Material Systems and Structures, 19: 651-669.

Riche, L. R. and Haftka, R. T., 1993, "Optimization of laminate stacking sequence for buckling load maximization by genetic algorithm," AIAA Journal, 31(5):951–956.

Captures for figures and tables

Figures

Figure 1 The coordinate systems $O - xyz$ for the laminated composite considered here.

Figure 2 Finite element model for the present composite plate, and impulse input and accelerometer attached nodes used in calculations.

Figure 3 Block diagram of the present control system.

Figure 4 The ith actuator with end point nodes $p^{(i)}{}_1$ and $p^{(i)}{}_2$, and forces by actuator.

Figure 5 Design process of the optimization proposed here.

Figure 6 Optimum actuator placements for plates with the optimum lay-up [0/0/0/0]s and specified lay-ups [0/-45/45/90]s, [45/-45/45/-45]s and [0/90/0/90]s.

Figure 7 Constitution of the experimental set up

Figure 8 Placement of actuators, accelerometer and impulse input for the [0/0/0/0]s plate used in the experiment.

Figure 9 Calculated and measured accelerances for the plate with two PZT actuators (suppressing the 1st and 2nd modes vibration).

Figure 10 Optimum actuator placements on the plates with optimized lay-ups and different numbers of actuators.

Figure 11 Accelerances for the [-15/-15/0/-45]s (optimum) and [0/0/0/0]s plates with the optimum actuator placements (AC = 2) (suppressing the 1st, 2nd and 3rd modes vibration).

Figure 12 The lowest three vibration modes and actuator placements for the [-15/-15/0/-45]s and [0/0/0/0]s plates.

Tables

Table 1 Properties of PZT actuators used in this study.

Table 2 Results of the present optimization with commonly used lay-up configurations and the actuator placement optimization for specified lay-up configurations (suppressing the 1st and 2nd modes vibration).

Table 3 Results of the present optimization with fine increment angles for plates with different numbers of actuators (suppressing the 1st, 2nd and 3rd modes vibration).

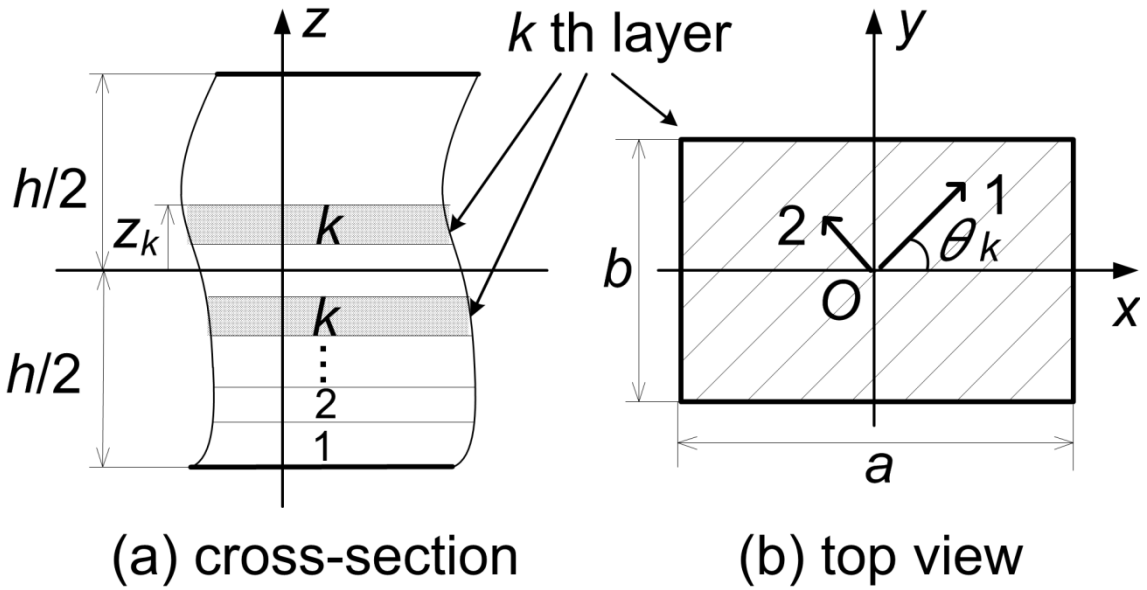

Figure 1 The coordinate systems *O* – *xyz* for the laminated composite considered here.

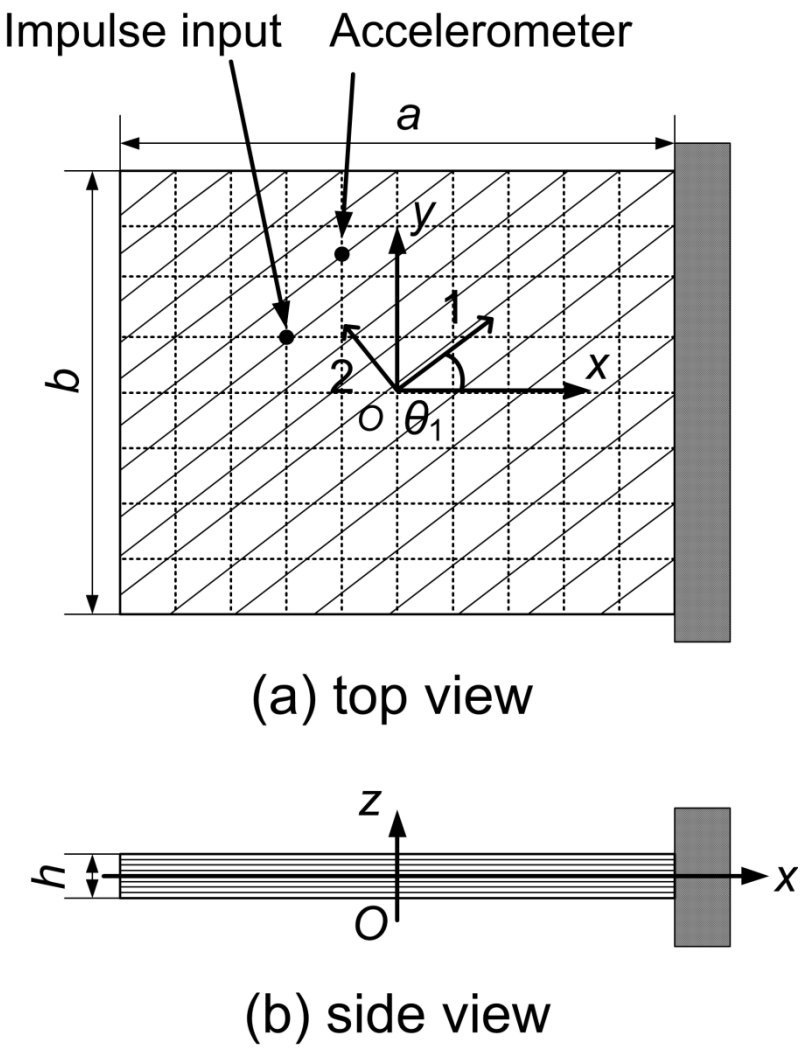

Figure 2 Finite element model for the present composite plate, and impulse input and accelerometer attached nodes used in calculations.

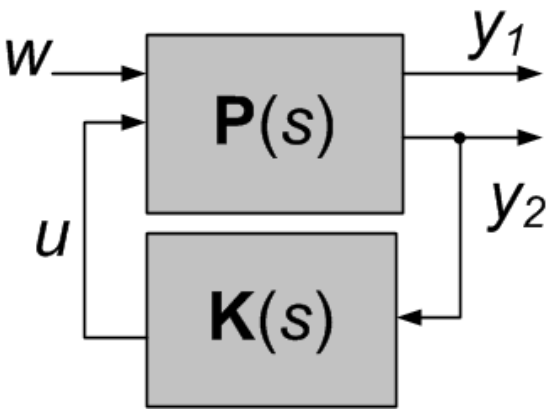

Figure 3 Block diagram of the present control system.

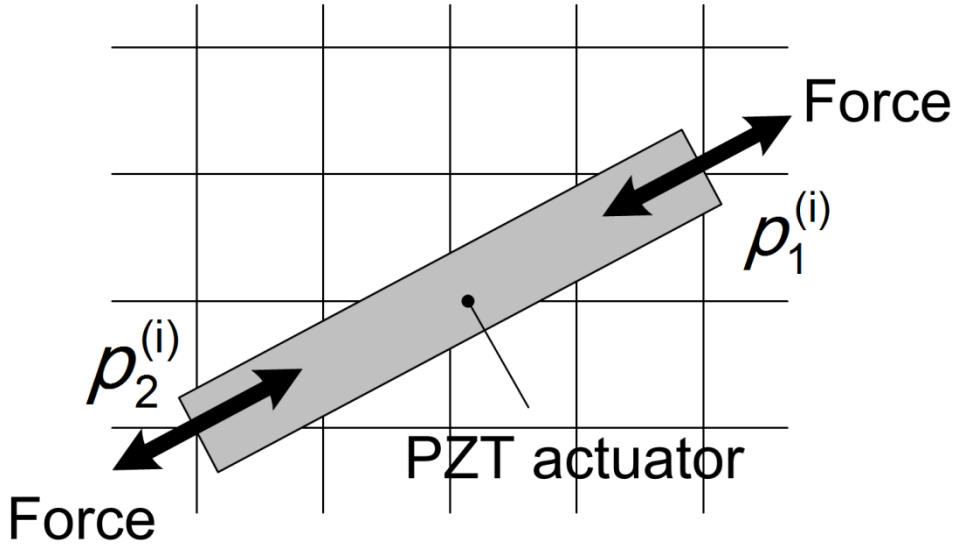

Figure 4 The *i*th actuator with end point nodes $p^{(i)}{}_1$ and $p^{(i)}{}_2$, and forces by actuator.

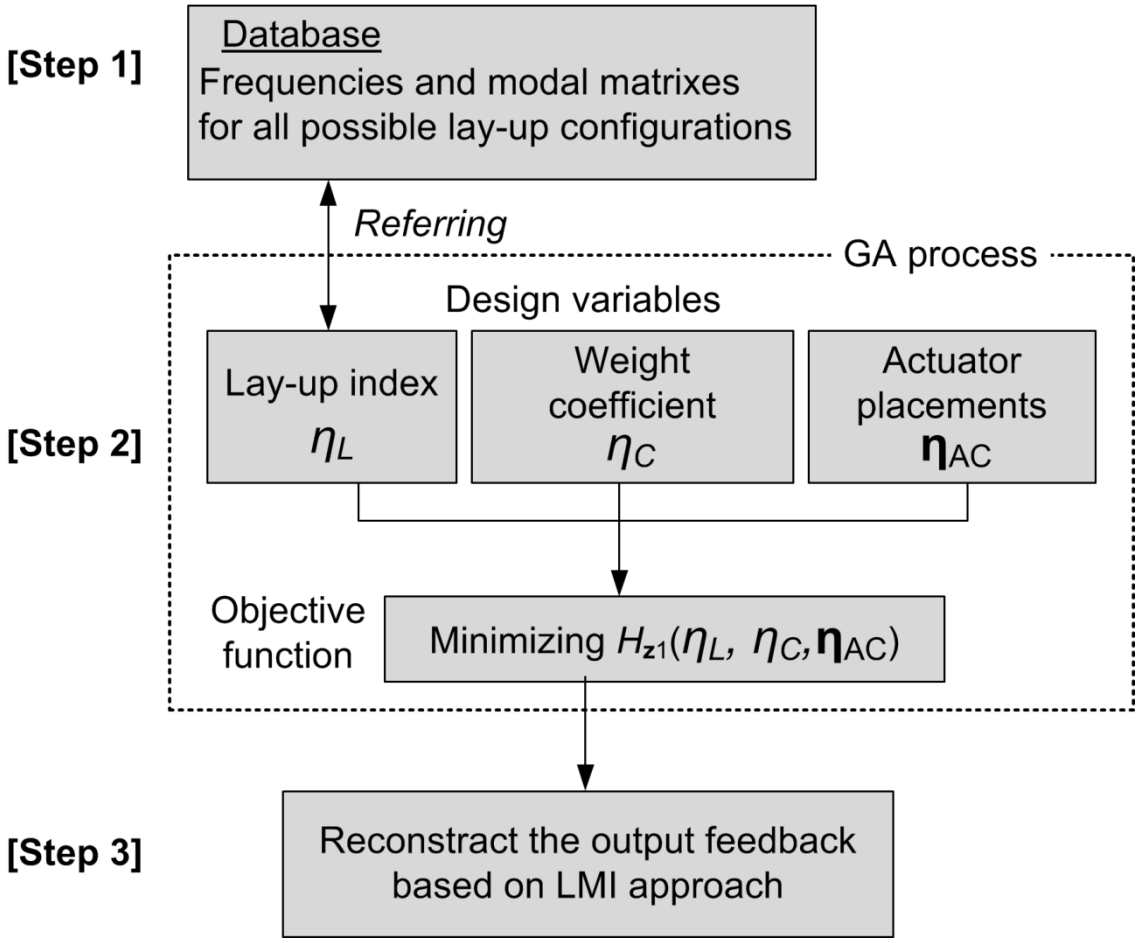

Figure 5 Design process of the optimization proposed here.

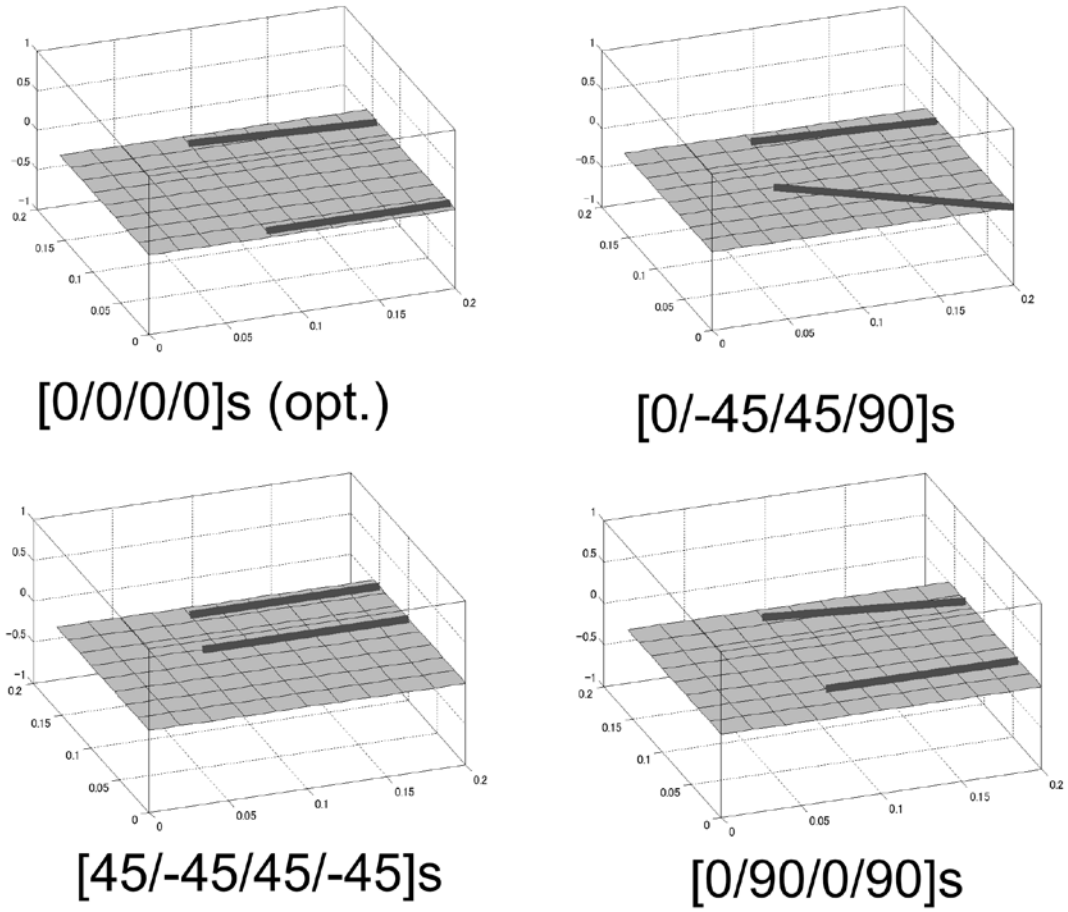

Figure 6 Optimum actuator placements for plates with the optimum lay-up [0/0/0/0]s and specified lay-ups [0/-45/45/90]s, [45/-45/45/-45]s and [0/90/0/90]s.

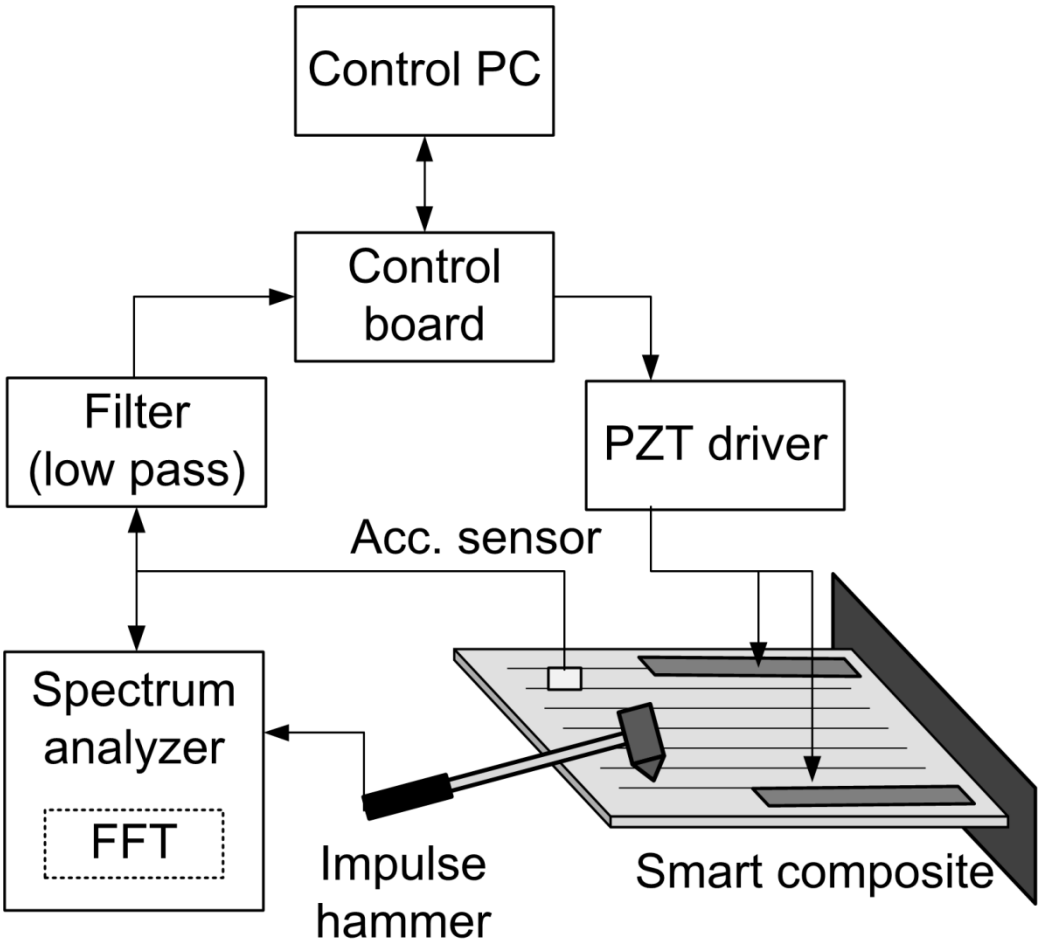

Figure 7. Constitution of the experimental set up

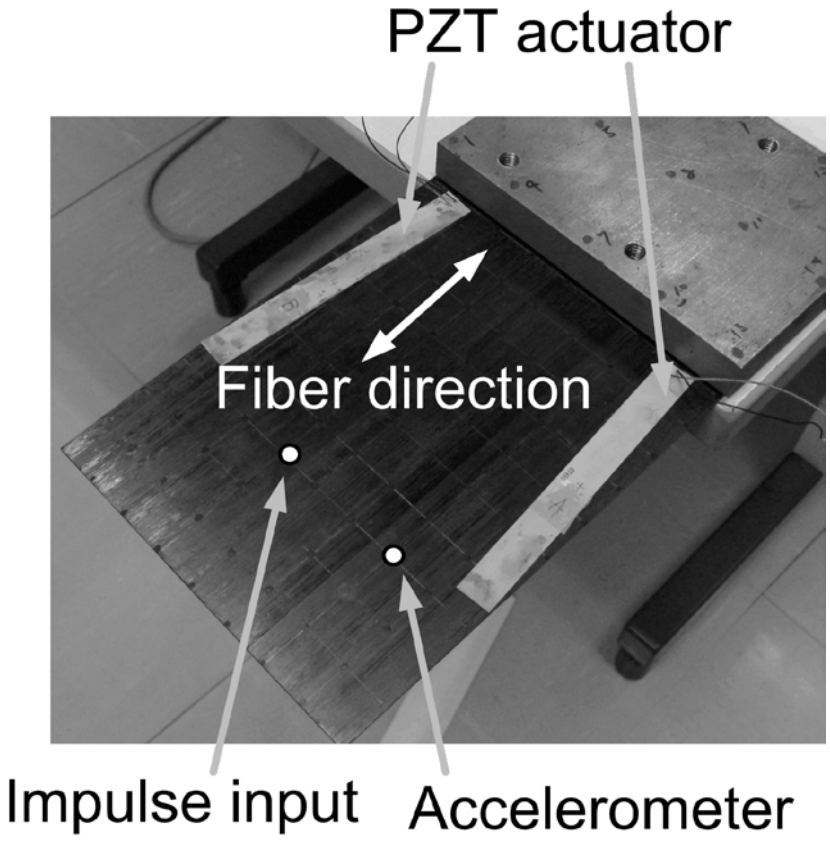

Figure 8 Placement of actuators, accelerometer and impulse input for the [0/0/0/0]s plate used in the experiment.

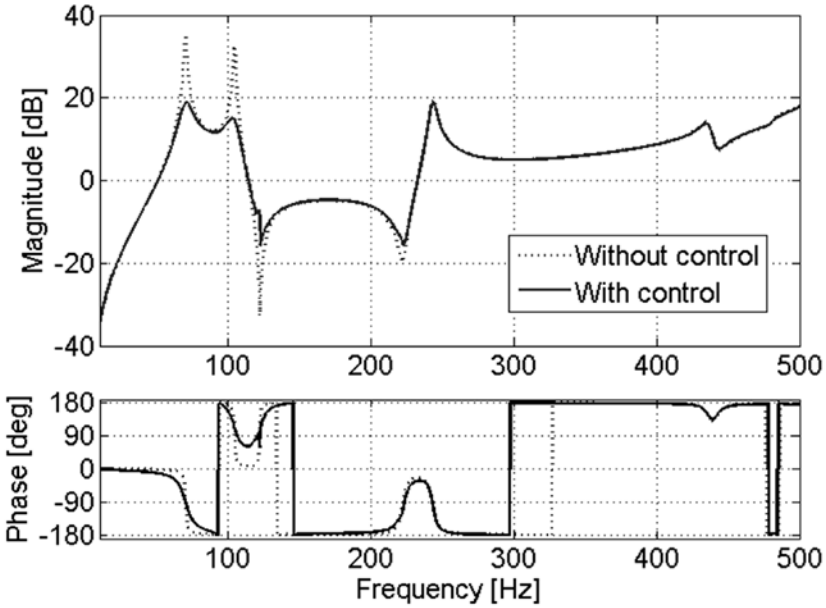

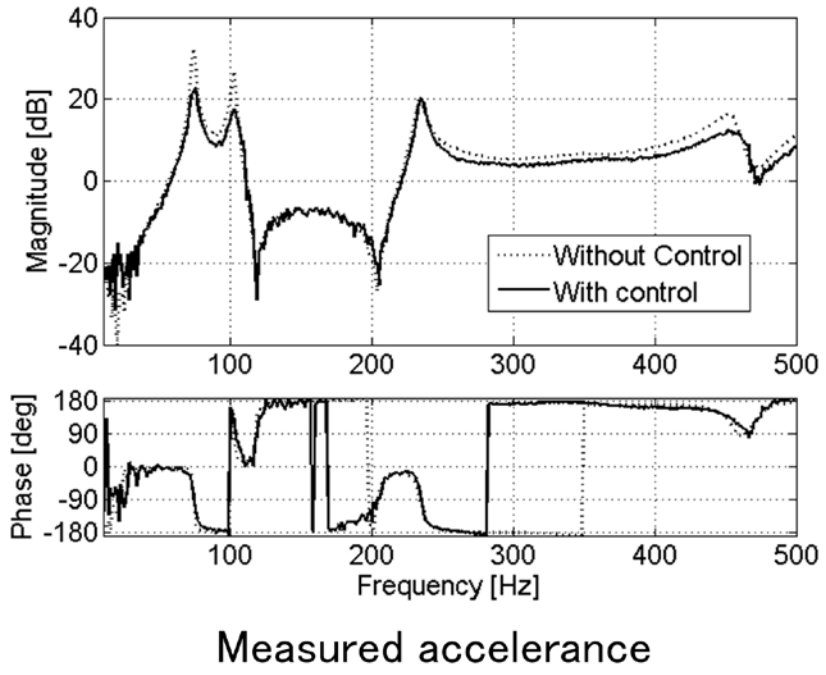

Figure 9. Calculated and measured accelerances for the plate with two PZT actuators (suppressing the 1st and 2nd modes vibration).

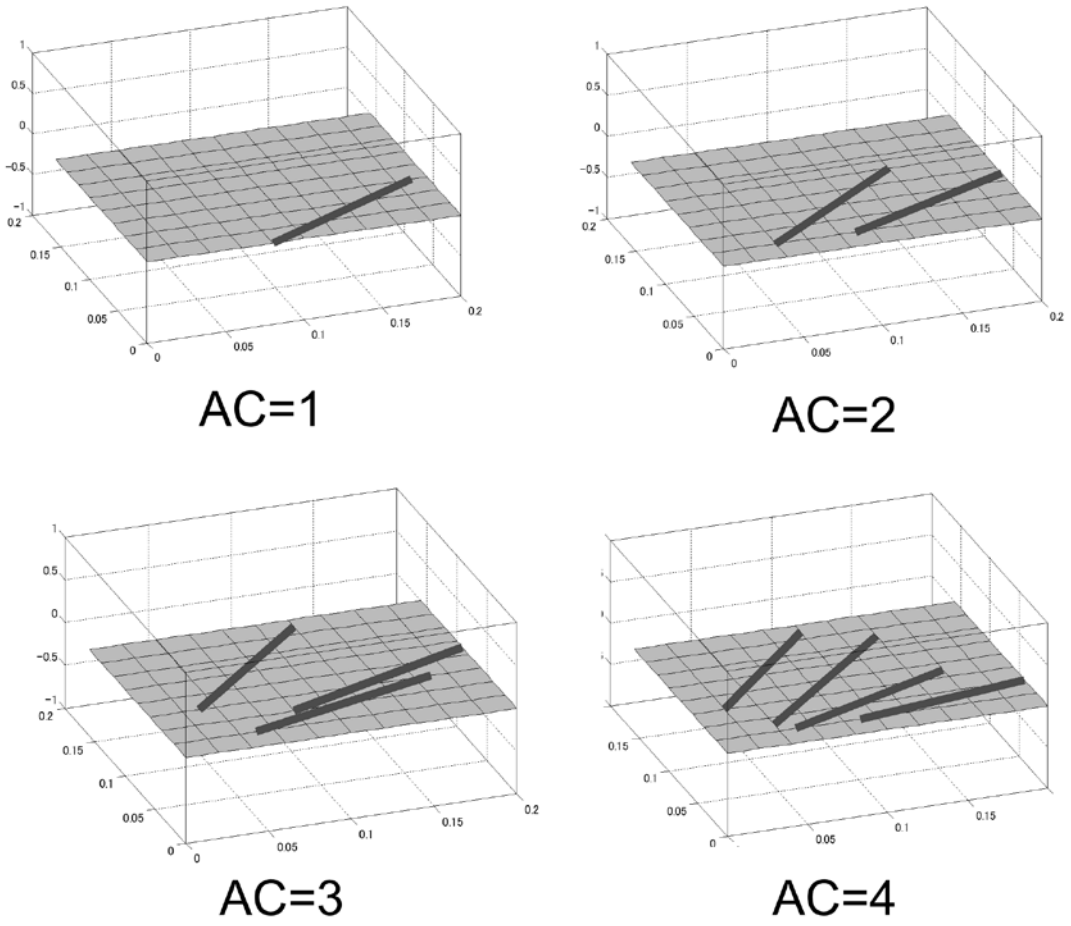

Figure 10 Optimum actuator placements on the plates with optimized lay-ups and different numbers of actuators.

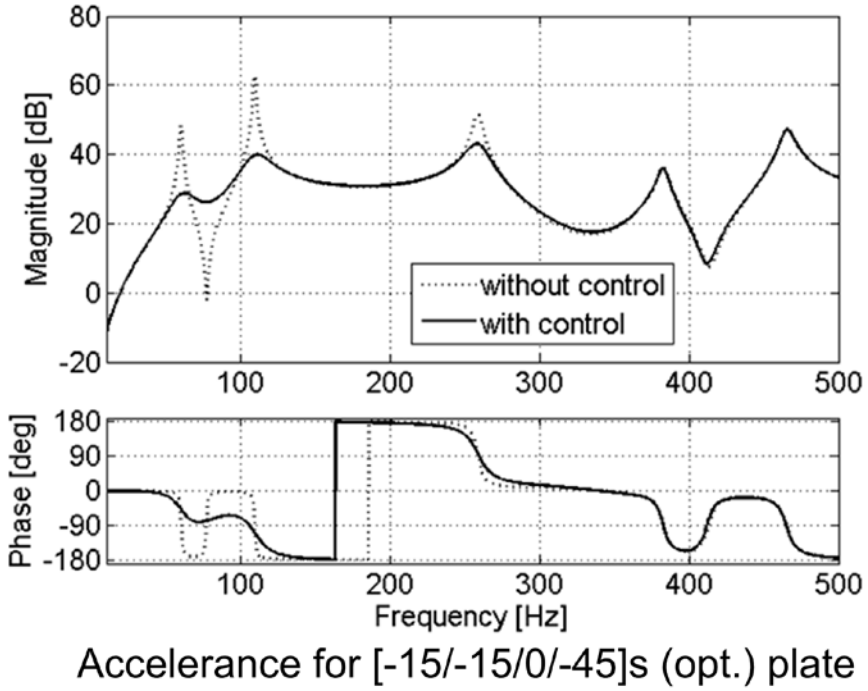

Accelerance for [-15/-15/0/-45]s (opt.) plate

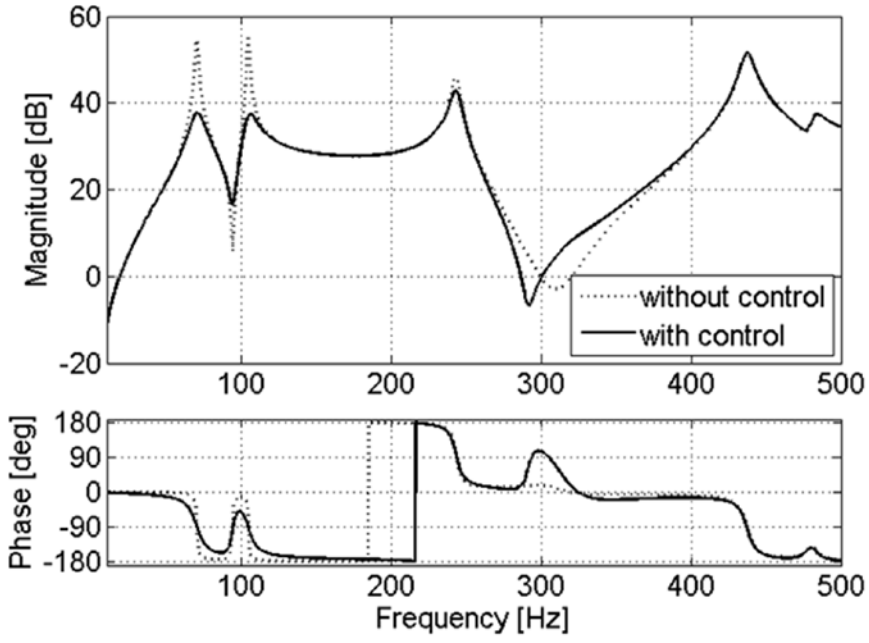

Accelerance for [0/0/0/0]s plate

Figure 11 Accelerances for the [-15/-15/0/-45]s (optimum) and [0/0/0/0]s plates with the optimum actuator placements (AC = 2) (suppressing the 1st, 2nd and 3rd modes vibration).

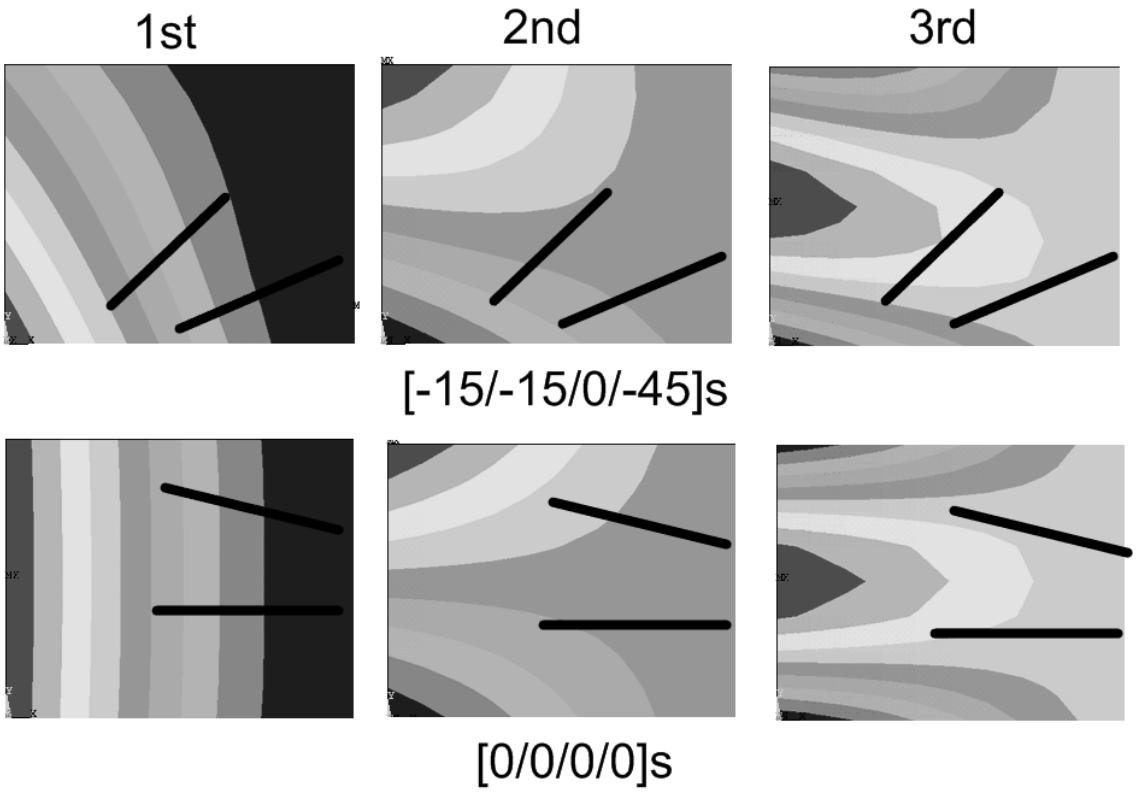

Figure 12 The lowest three vibration modes and actuator placements for the [-15/-15/0/-45]s and [0/0/0/0]s plates.

Table 1 Properties of PZT actuators used in this study.

Material properties	Values
Young's modulus, E (GPa)	62
Poisson's ratio, v	0.32
Density, ρ (kg/m^3)	7650
Thickness (m)	0.0005
Width (m)	0.015
Length (m)	Variable (≤ 0.13)
Piezoelectric coefficients	**Values**
d31 (m/V)	-210×10^{-12}
d33 (m/V)	472×10^{-12}
d15 (m/V)	758×10^{-12}

Table 2 Results of the present optimization with commonly used lay-up configurations and the actuator placement optimization for specified lay-up configurations (suppressing the 1st and 2nd modes vibration).

Lay-up	H_{z1} (x 10^{-7})	q_w (x 10^{7})
[0/0/0/0]s (opt.)	6.76	2.00
[45/-45/45/-45]s	26.2	0.400
[0/45/-45/90]s	9.79	1.30
[0/90/0/90]s	9.88	1.30

Table 3 Results of the present optimization with fine increment angles for plates with different numbers of actuators (suppressing the 1st, 2nd and 3rd modes vibration).

AC	q_w (x 10^7)	H_{z1} (x 10^{-7})	H_u	Opt. lay-up
1	2.60	6.01	0.10	[-15/-15/0/-45]s
2	3.50	4.42	0.10	[-15/-15/0/-45]s
3	4.60	3.71	0.10	[-15/-15/0/-45]s
4	6.00	3.27	0.098	[-15/-15/0/-45]s